 doi:10.20944/preprints202206.0088.v1

Article

A comprehensive energy model for an optimal design of a hybrid refrigerated van

Angelo Maiorino[1,*], Adrián Mota-Babiloni[2], Fabio Petruzziello[1], Manuel Gesù Del Duca[1], Andrea Ariano[1] and Ciro Aprea[1]

[1] Department of Industrial Engineering, University of Salerno, Via Giovanni Paolo II 132, Fisciano, (SA) 84084, Italy; A.M., amaiorino@unisa.it, F.P., fpetruzziello@unisa.it, M.G.D.D, mdelduca@unisa.it, C.A., aprea@unisa.it

[2] ISTENER Research Group, Department of Mechanical Engineering and Construction, Campus de Riu Sec s/n, Universitat Jaume I, Castelló de la Plana E-12071, Spain; A.M.B., mota@uji.es

* Correspondence: A.M., amaiorino@unisa.it; Tel.: +39 (0) 89 964105

Abstract: The path towards decarbonization requires a progressive adaptation of all refrigeration systems, but only stationary ones have been intensely studied to improve their environmental performance. However, refrigerated transport is a vital piece of the cold chain, and it must be considered in the green transition. In this paper, we propose a model for a hybrid refrigerated van that includes photovoltaic panels and electric batteries to decrease total greenhouse gas emissions from the engine. Thermal, electrical, and battery sub-models are considered and integrated into the comprehensive hybrid solar-powered refrigerated van model. Different technologies are compared in economic terms, including Lithium and Lead-acid batteries and three different types of photovoltaic panels. The model was validated regarding van fuel consumption, showing a 4% deviation. Single and multiple delivery scenarios are considered to assess the energetic, economic, and environmental benefits. Monthly CO_2,e emissions could be reduced to 20% compared to a standard refrigerated van. Despite the environmental benefits provided by this sustainable solution, the payback period is still too long (above 20 years) because of the necessary investment to adapt the vehicle and considering fuel and electricity prices currently.

Keywords: Refrigerated transport; Photovoltaic panels; Electrical batteries; Thermal model; Cold chain; Carbon emissions

1. Introduction

The transport sector requires effective public interventions and measures to reduce CO_2,e (carbon dioxide equivalent) emissions and reduce the vulnerability to climate change. CO_2,e emissions from this sector are about 30% in developed countries of anthropogenic origin and 23% worldwide [1]. There are 4 million refrigerated road vehicles, and together with refrigerated containers and supermarkets, 45% of the electricity is consumed by refrigeration equipment [2]. Of that, 55% of the refrigerated road vehicles are vans, followed by semi-trailers and trucks (25% and 20%, respectively). CO_2,e emissions per kg of food and kilometer from refrigeration systems of the small vehicles are more than double the larger ones, for both chilled and frozen distribution of different products [3]. More than 98% of all foods within the UK are transported by road, and the distances traveled have increased in recent years [4]. Tertiary distribution using rigid vehicles was the most energy-intensive transportation method, while primary distribution at ambient temperature was the least.

Refrigerated transportation, which is more intensive than stationary refrigerated systems, has also increased during the past years. Overall CO_2 emissions of vans with refrigeration units are 15% higher than standard vehicles, with NO_x emissions estimated to rise by 18%. The weight of the additional engine in the transport refrigerated sector is

Preprints (www.preprints.org) | NOT PEER-REVIEWED | Posted: 6 June 2022 doi:10.20944/preprints202206.0088.v1

significant [5]. Sovacool et al. [6] highlighted the transport and delivery sector as one of the most carbon-intensive emissions of the food and beverages industry. A major improvement suggested was the uptake of distributed generation and small-scale renewable energy systems. It is one of the three most significant areas with higher energy and carbon savings potential.

Compared to other refrigeration systems, refrigerated transport has not focused on the transition to lower environmental impact refrigerants [7]. Li [8] determined a theoretical reduction in CO_2,e emissions between 5% and 15% in a refrigerated trailer when replacing R404A with R452A. Citarella et al. [9] carried out a thermo-economic and environmental analysis in which R452A presented low set-up costs and high COP in the optimal configuration, representing a good compromise as mid-term R404A replacement. Górni et al. [10] confirmed the suitability of a method for assessing lubricity of POE with R404A and R452A, essential in the selection of oil for new refrigerants and long-life refrigeration systems with low energy consumption.

Nasuta et al. [11] developed an Excel-based Life Cycle Climate Performance calculation tool for transport refrigeration and bus air conditioning applications. They proved that indirect emissions (for electricity generation) dominate total emissions. Tassou et al. [12] identified several ways to reduce energy consumption in refrigerated transport, such as utilizing the exhaust heat, utilizing phase change materials, or hybridizing system arrangements and recommended further investigation into solar energy-driven systems. Wu et al. [13] determined that CO_2,e emissions caused by the energy consumption to power the compressor and carry the refrigeration unit resulted in large part of the total. Moreover, refrigerators driven by auxiliary engines have higher CO_2,e emissions than those operated by the vehicle engine or electricity.

Cenex [14] included electrification as one of the cleaner options for the future, replacing the auxiliary diesel engine with electricity from a battery, fuel cell, or even a solar photovoltaic (PV) array to run the refrigeration compressor. Njoroge et al. [15] state that renewable energies powering refrigeration systems must be installed to transport perishable goods. The solar PV array is mounted on the top of the vehicle, whereby an inverter system is used to convert the DC output to AC. Excess energy is stored in the batteries to supplement any shortfall. A few patents have been registered with PV technology. Blasko et al. [16] included a power management controller to select from two electrical power sources to power two motors (compressor and fan).

Solar refrigeration technology comprises a compound system in which solar power produces cold [17]. Solar PV cooling (also known as solar-assisted vapor compression refrigeration) shall consist of four essential components: PV modules, a battery, an inverter circuit, and a vapor compression system. Lazzarin [18] identified comparable costs between the PV-driven system concerning the solar thermal. Although the specific cost of PV is well higher than solar thermal, it is lowering, and their efficiency is improving continuously. Infante Ferreira and Kim [19] agreed that vapor compression cycles combined with PV collectors lead to the economically most attractive solutions. According to Kim and Infante Ferreira [20], the most significant advantages of PV panels combined with conventional vapor compression systems are simplicity and relatively high overall efficiency. However, drawbacks like the necessity of batteries (thermal or electrical) and the price of PV panels prevent the extension of these systems.

Salilih and Birhane [21] proved that solar radiation intensity increases the compressor rotational speed when directly connected to PV panels. Its energy performance, cooling capacity, or power consumption are also variable; therefore, a battery can decouple refrigeration parameters from the solar intensity. Su et al. [22] confirmed this assumption experimentally and emphasized the influence of ambient temperature on the cooling capacity and energy performance.

PV-driven refrigeration has not been extensively studied in refrigerated transport, but it presents promising results in other refrigeration, air conditioning, and heat pump applications. Mahmoudi et al. [23] studied a 170 m^2 PV integration for a cold storage facility, and the energy consumption decreased by around half, with a 5.2 years payback

Preprints (www.preprints.org) | NOT PEER-REVIEWED | Posted: 6 June 2022 doi:10.20944/preprints202206.0088.v1

period. Novaes Pires Leite et al. [24] found robust techno-economic viability in integrating air-conditioning and solar PV systems, especially in tropical latitude regions. Essential variables are energy price, annual adjustment, PV cost, and solar panel efficiency.

PV refrigeration has been compared usually with other cooling technologies, showing benefits in different aspects. Regarding costs of investment, Lazzarin and Noro [25] found PV-driven technologies because they offer similar cooling production at the expense of about half that of the best thermally driven system. The unexpected drop in PV module costs changed completely the competition between thermally or electrically driven solar cooling systems. Reda et al. [26] proved that the PV-driven heat pump is more economically viable than solar absorption for office building applications in the Northern climate. Riva et al. [27] concluded that PV-driven systems present almost half CO_2,e emissions compared to solar absorption heat pumps, and economies of scale offer opportunities to improve them.

Refrigerated transport must reduce greenhouse gas emissions to meet global sustainable targets. However, they are still strongly dependent on fuel consumption. A few past works have proved how refrigeration systems can be efficiently powered by solar energy, but this is not studied in detail in refrigerated transport, where other parameters, such as weight, become vital for the resulting CO_2,e emissions. From a thermal, energetic, and economic perspective, this work aims to model and analyze an innovative hybrid refrigerated van equipped with a PV system that powers the refrigeration unit. Moreover, the renewable source is sized considering different PV technologies. The charge and discharge curves are evaluated as a function of the required cooling load, batteries capacity, impact of temperature on performance, and comparison between lithium and lead-acid batteries.

2. Comprehensive energy model

A comprehensive energy model was developed to optimize the design of a photovoltaic system coupled to the refrigeration unit of a commercial van to reduce energy consumption and CO_2,e emissions (Figure 1). A photovoltaic system to provide a gross peak power of 600 W was considered for this investigation. The main characteristics of the van and the photovoltaic system can be found in Appendix A.

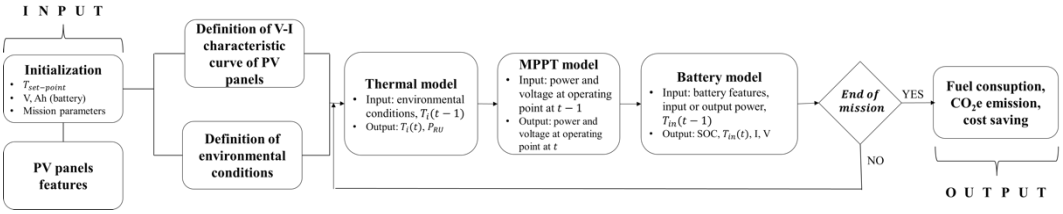

Figure 1. Model flow diagram.

The energy model is composed of several sub-models. The first is the thermal model (detailed equations can be found in Appendix B). It has the objective of evaluating the internal temperature of the cold room using transitory boundary conditions and the required cooling power. The thermal model is based on a heat balance equation with lumped parameters, Equation (1).

$$m_{in}c_{in}\frac{\partial T_{in}}{\partial t} = \dot{Q}_{aux} + \dot{Q}_{defrost} + \dot{Q}_{door} - \dot{Q}_{RU} + \dot{Q}_{in-w} + \dot{Q}_{in-c}, \quad (1)$$

where m_{in}, c_{in} and T_{in} are the mass, the specific heat capacity, and the air temperature inside the cold vain, respectively. $\dot{Q}_{aux}$, $\dot{Q}_{defrost}$ and $\dot{Q}_{door}$ are the thermal loads due to the auxiliary components, the defrost cycle, and the door opening, respectively, $\dot{Q}_{RU}$ is the cooling power, $\dot{Q}_{in-w}$ and $\dot{Q}_{in-c}$ are the thermal loads due to the heat exchange with the walls and the cabinet, respectively. The initial conditions are calculated for any external condition (airspeed, irradiance, temperature), considering the case in which the temperature profile in the walls follows a hysteretic cycle. This cycle oscillates around the set-

Preprints (www.preprints.org) | NOT PEER-REVIEWED | Posted: 6 June 2022 doi:10.20944/preprints202206.0088.v1

point air temperature following the refrigeration ON/OFF cycle. Figure 2 represents the thermal fluxes to which the cold chamber is subjected.

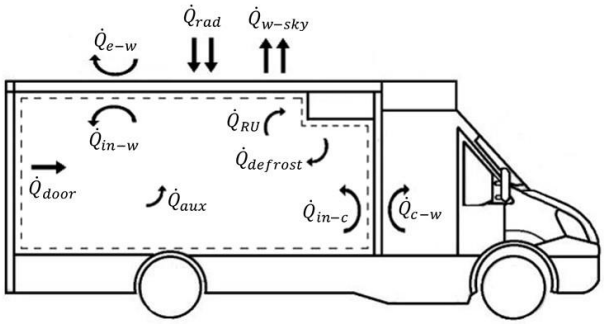

Figure 2. Heat flow schematic.

The first validation of this sub-model was carried out with an experimental test in static mode performed in March 2020. The electric power absorbed by the refrigeration unit and air temperature at the inlet and outlet of the evaporator was measured. The inputs were the external conditions, temperature and speed of the internal/external air, irradiance (obtained by the PVGIS-SARAH database), set-point temperature, and initial operating conditions. According to the targeted internal and external conditions, three cooling levels can be set in the vehicle. These are maximum cooling power during the pull-down stage, an intermediate operation when the system is switched on during hysteresis cycles, and a minimum level regulating the power supply frequency.

According to an MPPT (Maximum Power Point Tracking)-based logic, the model identifies the amount of power provided by the PV system, the one supplied or absorbed by the battery, and the one provided by the van's internal combustion engine.

A battery model (Appendix C) provides the State of Charge (SOC) and the voltage (V) of the battery. Two different behaviors were considered for lithium and lead-acid battery, both in the charging and discharging phase.

The cumulation of the results provided by the model during an extended period allows to calculate the associated fuel consumption and CO_2,e emission, together with the value of the electricity losses at the PV panels, battery (electrical connections), refrigeration unit, inverter, and relative savings in electricity over the entire month, excluding the battery charge. Fuel consumptions due to van traction and power refrigeration system depend on the specific route. The input data are the time of arrival at each checkpoint (points at which the parameters are evaluated and then kept constant until the next checkpoint), average speed of the van, distance between two successive checkpoints, and load carried.

The CMEM (Comprehensive Modal Emission Model) approach [28], used to estimate the fuel consumption and emissions related to the vehicle's operation, is based on several parameters that vary according to the specific vehicle, engine, and operation considered. Most of these parameters are related to the vehicle and the engine characteristics (engine size, vehicle mass and frontal area, aerodynamic drag coefficient) and are easily obtainable. For example, other parameters refer to vehicle operation and can be deduced through ECU readings. Such a method is called "comprehensive" as it can be applied to all the vehicles. Based on this approach, the instantaneous rate of fuel consumption $\boldsymbol{FR}$ when traveling at a constant speed $\boldsymbol{v}$ with a specific load $\boldsymbol{l}$ is estimated using Equation (2).

$$\boldsymbol{FR} = \frac{\xi}{\boldsymbol{LHV_{fuel}\rho_{fuel}}}\left(\boldsymbol{kN_{en}D_{en}} + \frac{\boldsymbol{0.5C_d\rho Av^3}+(\mu+l)v(g\sin\Phi)+gC_r\cos\Phi}{\boldsymbol{1000\eta_{mec}\eta_g}}\right), \quad (2)$$

where $\boldsymbol{\xi}$ is the mixture ratio, $\boldsymbol{LHV_{fuel}}$ lower heating value of the fuel, $\boldsymbol{\rho_{fuel}}$ density of the fuel, $\boldsymbol{k}$ engine friction factor, $\boldsymbol{N_{en}}$ engine rotation speed, $\boldsymbol{D_{en}}$ engine displacement, $\boldsymbol{C_d}$ coefficient of aerodynamic drag, $\boldsymbol{\rho}$ air density, $\boldsymbol{A}$ area of the front surface of

Preprints (www.preprints.org) | NOT PEER-REVIEWED | Posted: 6 June 2022 doi:10.20944/preprints202206.0088.v1

the van, v speed of the van, μ system weight (panels + battery + inverter), $\boldsymbol{l}$ transport load; g acceleration due to gravity, Φ street angle, C_r Rolling resistance coefficient, $\boldsymbol{\eta_{mec}}$ vehicle transmission efficiency, $\boldsymbol{\eta_g}$ overall efficiency of the internal combustion engine.

The fuel consumption $\boldsymbol{F}$, for a distance ($\boldsymbol{d}$) and certain speed ($\boldsymbol{v}$), is then calculated as Equation (3) shows.

$$\boldsymbol{F = FR\frac{d}{v}}. \quad (3)$$

The total fuel consumption of the trip is given by the sum of the consumptions in the single i-th sections, Equation (4).

$$\boldsymbol{F_{tot} = \sum_i F_i}. \quad (4)$$

Considering a conversion factor equal to 1.5 kg dm^{-3}, a unit cost of methane Cu of 0.99 € per kg and an emission factor f of 55.82·10^{-3} kgCO_2e MJ^{-1}, the cost and carbon footprint of the trip can be obtained from Equation (5) to (7).

$$\boldsymbol{m_{fuel,drive} = F_{tot}/1.5}, \quad (5)$$

$$\boldsymbol{C_{drive} = m_{fuel,drive}Cu}, \quad (6)$$

$$\boldsymbol{m_{CO_2,drive} = f\ LHV_{fuel}m_{fuel,drive}} \quad (7)$$

On the other hand, the fuel consumption due to the operation of the refrigeration unit is given by Equation (8).

$$\boldsymbol{m_{fuel,RU} = \frac{P_{RU}}{LHV_{fuel}\eta_{real}}}, \quad (8)$$

where $\boldsymbol{P_{RU}}$ is the electric power absorbed by the refrigeration unit without considering the PV generation, and $\boldsymbol{\eta_{real}}$ efficiency of the internal combustion engine, fixed at 20%, can be changed and made variable according to the operating conditions.

The model was validated considering a test carried out in early March 2020, during which the total fuel consumption was recorded. It involved a single delivery transport of 150 kg of frozen pastry products at a temperature of –20 °C. The comparison of the results obtained with the model and measurements is shown in Table 1.

Table 1. Comparison between measured data and results obtained from the model.

Parameter	Model	Test
Total distance (km)	90.2	
Total time (min)	63	
Departure	11.10	
Drive (kg)	10.02	Not applicable
Refrigeration (kg)	0.46	Not applicable
Total consumption (kg)	10.5	10.1
Total cost (€)	9.96	10.0
Total CO_2 emissions (kg)	28.1	28.2

The model obtains a 4% increase in consumption compared to the test (evaluated by OBD scanner). This error can be considered acceptable in an initial modeling and simulation phase.

3. Results and discussion

The potential of the innovative refrigerated van requires validation using real routes. Two situations were proposed. The first is a single delivery scenario characterized by a single trip from the production or distribution center to the point of sale. The second is a multiple deliveries scenario in which three points of sale were considered, assuming that the refrigerated products unloading operations last 10 minutes. Both also consider returning to the origin with the refrigeration unit off (all product is delivered). At the origin, the battery that powers the refrigeration unit is connected to an external electrical outlet to be

Preprints (www.preprints.org) | NOT PEER-REVIEWED | Posted: 6 June 2022 doi:10.20944/preprints202206.0088.v1

fully charged for the following day. Moreover, the van performs one trip a day on weekdays.

The operating conditions depend on the path considered for the simulation and extracted from Google Maps and the PVGIS-SARAH database. The first provides the traveled distance and the vehicle's speed. At the same time, the second has been used to know solar radiation, ambient temperature, and wind speed, averaged over the previous three years.

Meneghetti and Ceschi [29] recommended selecting the route with the minimum fuel consumption for both traction and refrigeration. Energy savings are affected by the location of the sale points, departure time, number of deliveries per trip, seasonality, and location of the delivery network. The locations considered in the trips are shown in Table 2. For this investigation, the road O-D1 (72.1 km road distance) was chosen as the single-delivery scenario and O-D2-D3-D1-O (97.5 km road distance) for the multiple deliveries scenario.

Table 2. List of locations considered for the trips. All locations are in Campania, Italy.

Code	Address	Coordinates
O	Via Santa Maria La Neve, Tramonti (SA)	40.70, 14.66
D1	Via Benedetto Croce 63, Avellino (AV)	40.92, 14.78
D2	Corso Giuseppe Garibaldi 12, Castellammare di Stabia (NA)	40.70, 14.48
D3	Via Salvatore D'Alessandro 42, Nocera Inferiore (SA)	40.75, 14.63

3.1. Single-delivery scenario

This section analyses the results of the comprehensive energy model applied to the single-delivery scenario to find the optimal photovoltaic system design.

3.1.1. Selection of PV panels

In the first step, three different models of PV panels are considered (their main characteristics can be found in Table A3 - Appendix A), assuming the system employs a 100 Ah 24 V lead-acid battery. Type A requires 327.3 kWh of energy from the power grid in a year to charge the battery before each departure. Model B requires 341.4 kWh, and model C requires 324.4 kWh, implying that model B has lower electricity production for a single trip.

Fig. 3 shows the energy produced by the three considered modules per month. The choice of PV panel does not significantly influence the total van weight, and consequently, the fuel consumption is not affected. The number of panels positioned on the roof, bound to the surface available, is calculated according to the necessary energy generated.

Preprints (www.preprints.org) | NOT PEER-REVIEWED | Posted: 6 June 2022 doi:10.20944/preprints202206.0088.v1

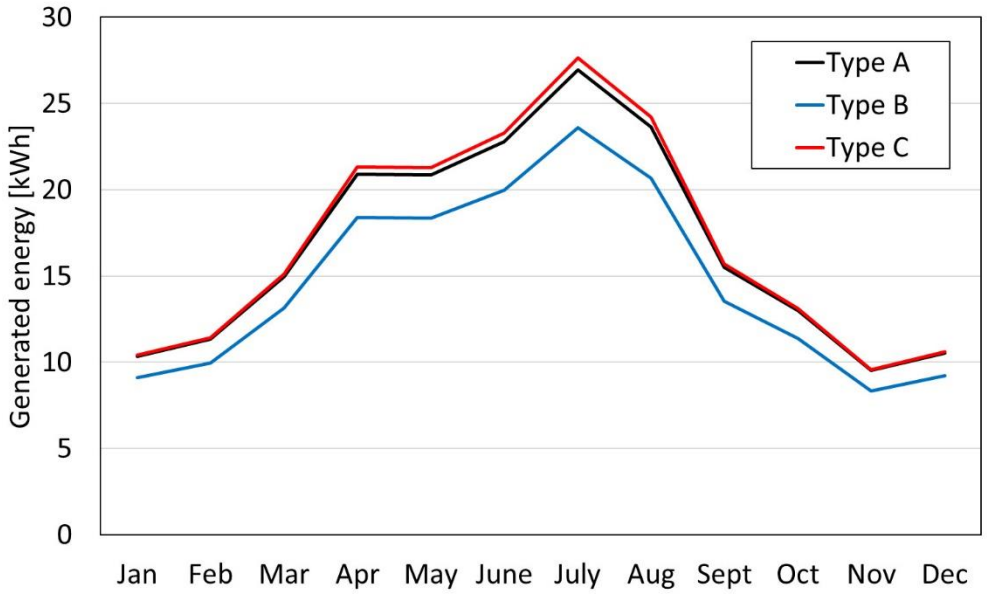

Figure 3. Energy generated by different PV modules.

The common costs for the PV system accessories are shown in Table 3, and the cost associated with each PV panel type is shown in Table 4. There is a significant difference in the cost among the different models, the more expensive, the higher production. Therefore, this analysis influences the payback period of the proposed solution. Moreover, it should be highlighted that the expected cost of any PV panel model represents between 25% and 43% of the final cost.

Table 3. Common costs for PV system accessories.

Component	Unit cost [€]	Units	Total cost [€]
MC4 connectors	4.80	1	4.80
Extension cable	1.20	14	16.80
Double-sided adhesive	18.00	5	90.00
Inverter-MPPT	473.72	1	473.72
24V 100Ah battery	480.00	1	480.00
Total			1065.32

Table 4. Investment required for each PV panel model.

PV model	Unit cost [€]	Units	Cost PV panels [€]	Total cost [€]
Type A	430.00	5	2150.00 €	3215.32
Type B	290.00	5	1450.00 €	2515.32
Type C	260.00	12	3120.00 €	4185.32

Attending to the costs and the electricity produced, a simulation is performed to evaluate the payback period of the different PV panel models, shown in Table 5, assuming a cost of the electricity from the power grid of 0.061 € per kWh. The PV panels reduce the annual costs of the van by about 7%. Still, the initial economic benefits are not considerable, so the payback period is not at an acceptable level, longer than a usual lifetime of a van. If necessary, the only model acceptable from an economic perspective in a refrigerated van doing single deliveries (one per day) would be model B, which could be compensated before replacing the refrigerated van. For this reason, model B was chosen as the best option for PV panel type, and therefore all the results presented after this were obtained considering only this model.

Preprints (www.preprints.org) | NOT PEER-REVIEWED | Posted: 6 June 2022 doi:10.20944/preprints202206.0088.v1

Table 5. Economic analysis.

Parameter	Baseline	Type A	Type B	Type C
Investment cost [€]	NA	3215.32	2515.32	4185.32
Power grid cost [€]	NA	19.97	20.82	19.79
Annual costs [€]	1606.46	1488.46	1492.68	1488.06
Net Present Value [€]	NA	118.00	113.78	118.40
Payback period [years]	NA	27	22	36

With the selected components, it is possible to evaluate to what extent the PV system can meet the electricity needs. Fig. 4 shows that the PV panels produce around half the energy required by the batteries for most of the months. The worst results for the months of winter. Moreover, the energy losses represent just a tiny percentage of the electricity produced.

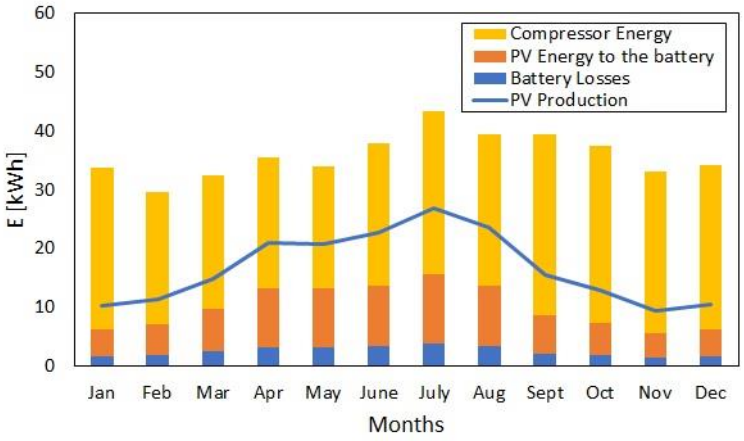

Figure 4. Monthly distribution of energy in the system: energy required to move the compressor of the refrigeration unit, energy produced by the PV panels and sent to the battery, battery losses, and total energy produced by the PV panels.

The electric power required by the refrigeration unit and the power generated by the PV panels are shown in a generic day for the previous route (see Fig. 5). As it can be seen, the compressor follows hysteretic cycles to keep the refrigerated compartment temperature at acceptable levels (Fig. 5a). Then, the power provided by the PV panels decreases from 0.37 to 0.30 kW because it is heated during the trip, and their efficiency is reduced (Fig. 5b).

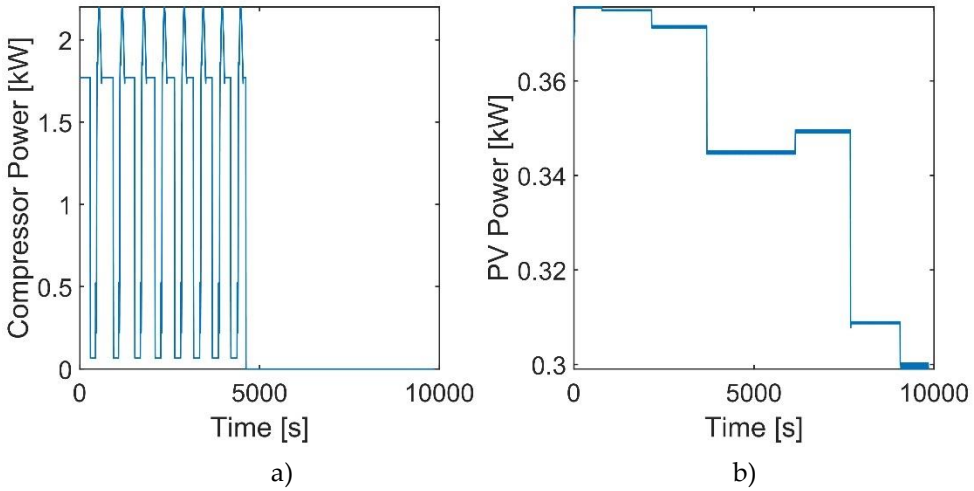

Figure 5. Power required by the refrigeration unit (left) and solar power available (right).

Preprints (www.preprints.org) | NOT PEER-REVIEWED | Posted: 6 June 2022 doi:10.20944/preprints202206.0088.v1

3.1.2. Selection of batteries

After comparing PV panel models, two types of batteries are analyzed, i.e., lead-acid and lithium. Fig. 6 presents current, voltage, state of charge (SOC), power, and temperature variations for the proposed single-delivery scenario. The lead-acid battery has more significant variations in terms of voltage, while the lithium battery is the one that presents a similar phenomenon according to the current. The SOC values of a lead-acid battery are always lower than lithium, while the power of both remains at comparable values. Finally, the lead-acid battery temperature is about 4 °C higher than lithium.

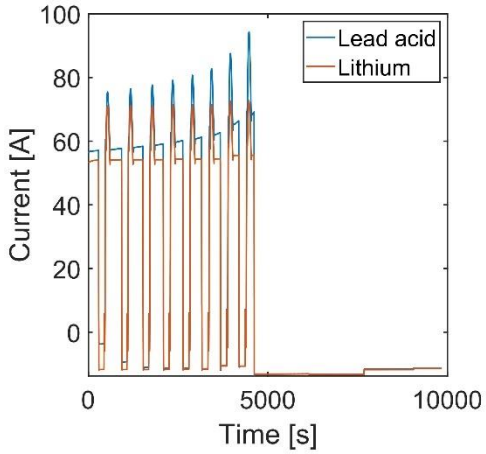

a)

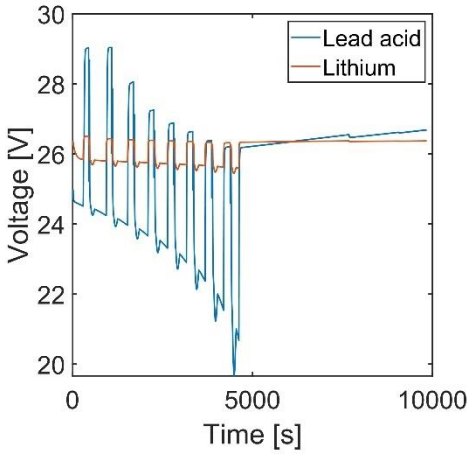

b)

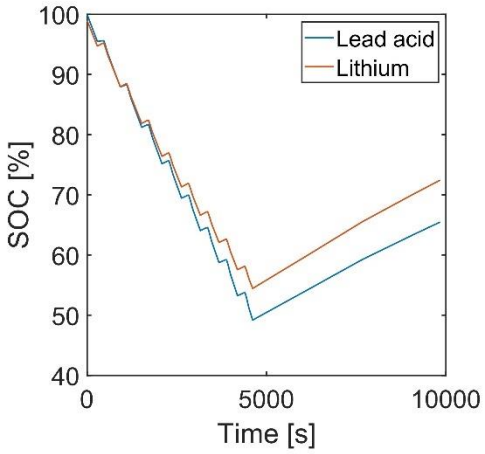

c)

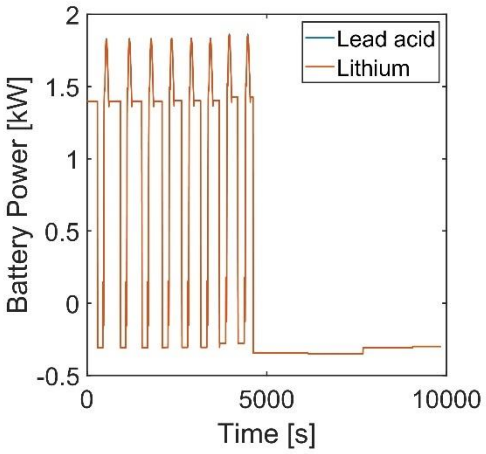

d)

Preprints (www.preprints.org) | NOT PEER-REVIEWED | Posted: 6 June 2022 doi:10.20944/preprints202206.0088.v1

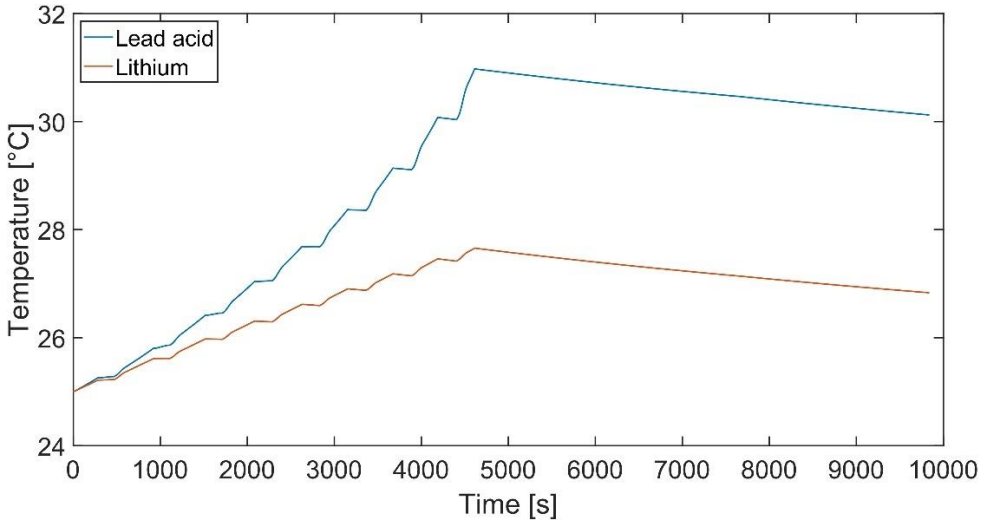

e)

Figure 6. Comparison of electrical and thermal behaviour between lead-acid and lithium battery: a) Current, b) voltage, c) SOC, d) power, and e) temperature.

Considering an economic analysis performed for the three types of PV panels, the payback period of each battery is analyzed, considering 670 € per kWh nominal for the lithium type and 200 € per kWh nominal for the lead-acid. Fig. 7 shows the payback period as a function of the capacity. It can be noticed that using a 100 Ah lead-acid battery allows for achieving the minimum payback period, which is 26 years. In contrast, for a lithium battery, the payback period is in constant increase, being the minimum of 28 years for 50 Ah capacity.

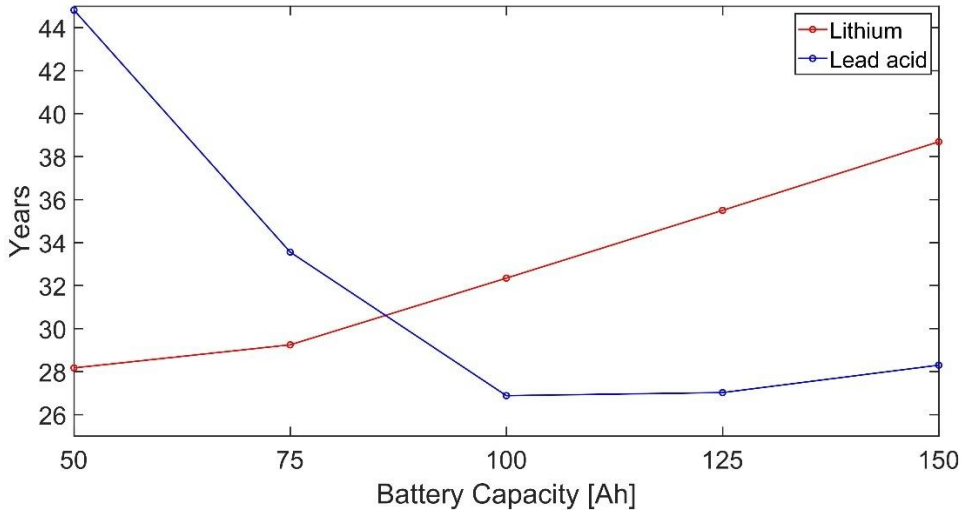

Figure 7. Behavior of the payback period of the lithium and lead-acid battery according to different capacities.

The Round Trip Efficiency (RTE) parameter is proposed for evaluating the suitability of the different batteries. Two parameters can be considered, one that only considers the amount of input and output energy at the battery (RTE_b) and another the available solar energy (RTE_{tot}). Both factors are added to the energy absorbed from the grid, as shown in Equations (9) and (10).

$$RTE_b = \frac{E_b}{E_{Reintegrated}+E_{PV-b}}, \quad (9)$$

Preprints (www.preprints.org) | NOT PEER-REVIEWED | Posted: 6 June 2022 doi:10.20944/preprints202206.0088.v1

$$RTE_{tot} = \frac{E_b}{E_{Reintegrated}+E_{sol-b}}, \quad (10)$$

where E_b is the energy provided by the battery to the refrigeration unit; $E_{Reintegrated}$ is the energy provided by the power grid to recharge the battery before the departure; E_{PV-b} is the energy provided by the photovoltaic system to charge the battery; E_{sol-b} is the available solar energy to recharge the battery. The difference between E_{PS-b} and E_{sol-b} is that E_{PV-b} is affected by the internal losses due to the efficiencies of the components.

The results are reported in Fig. 8 for lead-acid and lithium batteries for each month and different capacities.

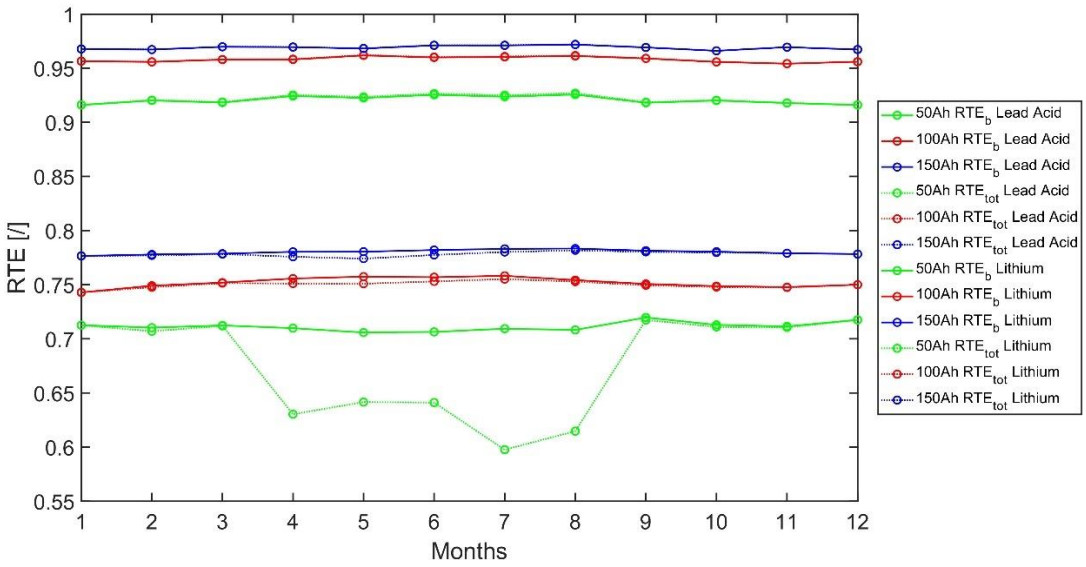

Figure 8. Comparison of RTE values among several battery solutions for both lead-acid and lithium types.

A 100 Ah lead-acid battery provides the best techno-economical compromise.

3.1.2. Overall results

Table 6 summarizes all information obtained per month for the final solution considered, i.e., model B as PV panel type and a 100 Ah 24 V lead-acid battery. This choice mainly comes from the economic analysis for the PV panels, whereas for the battery, some other factors were also considered (RTE). Savings refer to the economic savings evaluated by adopting the proposed solution concerning the original configuration of the van, considering that every day before the departure, the battery is fully charged by the grid. E_{RU} represents the energy absorbed by the refrigeration unit; E_{PS} is the energy provided by the photovoltaic system to run the refrigeration unit or recharge the battery; E_b is the energy supplied by the battery to run the refrigeration unit. Losses refer to energy losses attributed to each section of the photovoltaic power supply system.

Preprints (www.preprints.org) | NOT PEER-REVIEWED | Posted: 6 June 2022 doi:10.20944/preprints202206.0088.v1

Table 6. Monthly electric consumption in the scenario considered.

Parameter	Jan	Feb	Mar	Apr	May	Jun	Jul	Aug	Sep	Oct	Nov	Dec
Distance [km]						72.10						
Time [min]						77.00						
E_{RU} [kWh]	33.7	29.1	32.4	35.5	34.0	38.0	43.3	39.6	39.1	37.7	33.0	33.8
E_{PS} [kWh]	5.2	5.3	7.4	10.4	10.4	11.6	13.4	11.6	9.0	7.4	5.2	5.8
E_{bat} [kWh]	0.9	0.8	0.8	0.7	0.6	0.7	0.7	0.7	0.8	0.9	1.0	1.0
$E_{Reintegrated}$ [kWh]	30.4	24.0	26.4	23.9	21.9	24.7	24.8	24.9	26.6	30.6	29.1	31.8
$Losses_{PV}$ [kWh]	0.6	0.6	0.8	1.1	1.1	1.2	1.5	1.3	1.0	0.8	0.6	0.6
$Losses_{bat}$ [kWh]	0.1	0.1	0.1	0.1	0.1	0.1	0.1	0.1	0.1	0.1	0.1	0.1
$Losses_{RU}$ [kWh]	9.7	8.4	9.3	10.1	9.7	10.7	12.2	11.2	11.2	10.7	9.5	9.7
Losses inverter [kWh]	3.2	2.8	3.2	3.6	3.4	3.8	4.2	3.9	3.6	3.6	3.1	3.4
Losses tot [kWh]	13.6	11.8	13.4	14.9	14.3	15.9	18.0	16.4	15.7	15.5	13.2	13.8
Savings [%]	4.0%	12.1%	18.4%	32.8%	35.6%	34.9%	39.2%	30.4%	22.7%	12.9%	5.2%	5.7%

Fig. 9 shows the results that summarize the monthly electricity absorbed by the refrigeration unit, produced by the PV system, and reintegrated from the grid. The increase in fuel consumption for refrigeration in the summer months is slightly compared to the winter months. Refrigeration consumption is almost entirely cut thanks to the energy supplied by the battery connected to the PV panels, even if refrigerator energy consumption represents only 10% of total consumption.

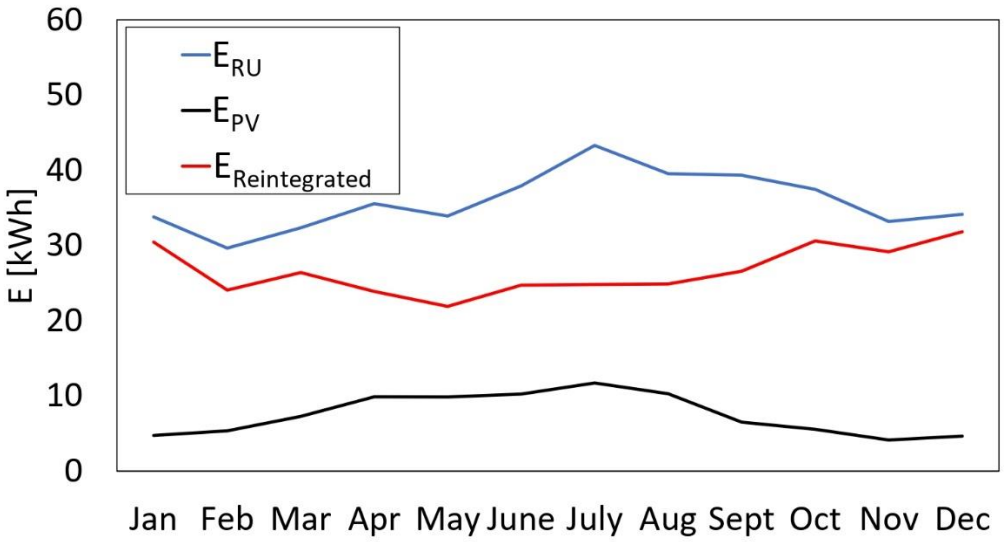

Figure 9. Monthly electricity absorbed by the refrigeration unit, produced by the PV system, and reintegration from the grid.

Fig. 10 depicts the economic and environmental feasibility of the proposed solution. Considering the single-delivery scenario presented, there is a total cost saving of about 100 € per year. Undoubtedly, the savings would be of no minor importance for longer trips and carrying out more than one trip per day. Furthermore, the economic saving is strongly affected by the unit cost of methane, and it should increase as the unit cost of methane increases. Therefore, a higher cost saving should be expected with an increasing unit cost of methane.

From the environmental perspective, it is possible to save in $CO_{2,e}$ emissions of about 150 to 250 kg per year; even in this case, the situation could improve considering longer trips and carrying out more than one trip per day.

Preprints (www.preprints.org) | NOT PEER-REVIEWED | Posted: 6 June 2022 doi:10.20944/preprints202206.0088.v1

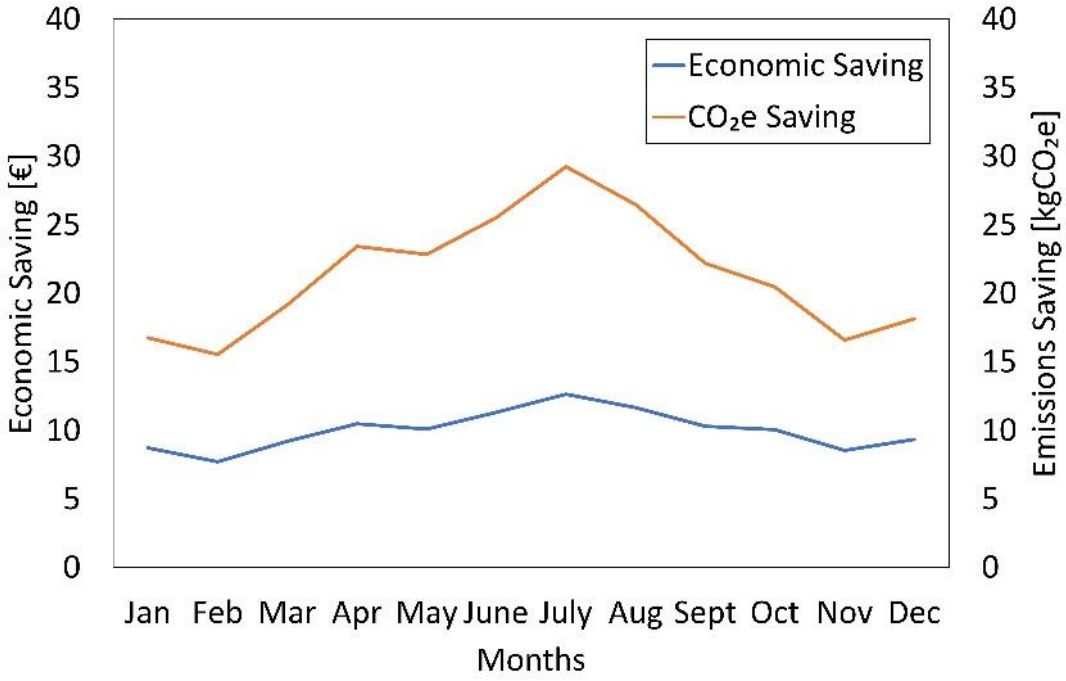

Figure 10. Monthly economic and CO_2 emissions savings provided considering single-delivery trips. The refrigerated van represents the reference solution without the PV panels installed.

3.2. Multiple-deliveries scenario

In this case, a route with multiple deliveries is considered, selecting the order of deliveries according to the most optimal route for minimizing the total distance and time traveled (which is not discussed since it is out of the aim of this work). Identifying the optimal design for PV panel and battery types is not performed since the single-delivery scenario was used to select the best solution. The same configuration was adopted to evaluate the performances in a multi-deliveries scenario.

Fig. 11 depicts that the electricity required by the cooling unit has a minimum variation throughout the year. A peak is observed in July, but the cooling demand is only approximately 30% higher than in February (Fig. 11a). The electricity taken from the grid represents between 50% and 63% of the total required. The electricity generated by the PV panels varies between 16% and 32% of the necessary cooling.

Moreover, there is a significant difference for the single-delivery scenario, represented by the heat gain due to the unloading operations of products considered in a multiple-deliveries scenario. The cooling required due to the air infiltration (opening the doors for charge/discharge load) represents between 23.5% and 33.6% of the total (Fig. 11b).

Preprints (www.preprints.org) | NOT PEER-REVIEWED | Posted: 6 June 2022 doi:10.20944/preprints202206.0088.v1

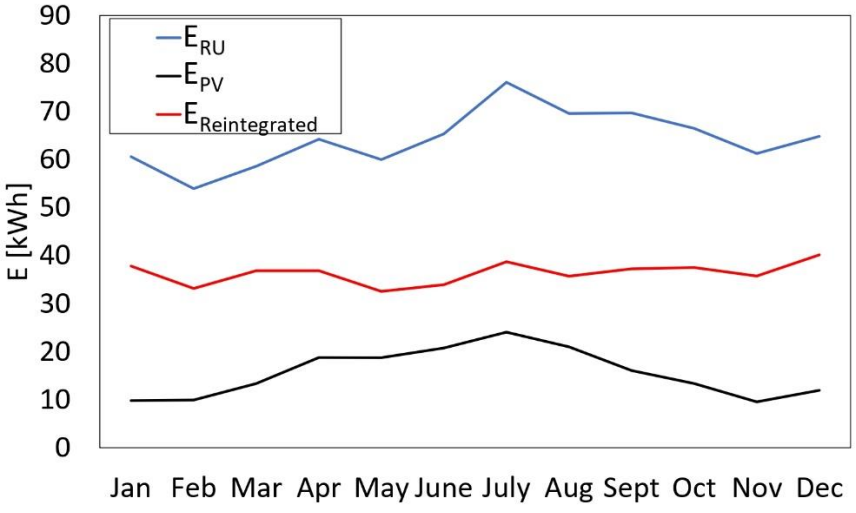

a)

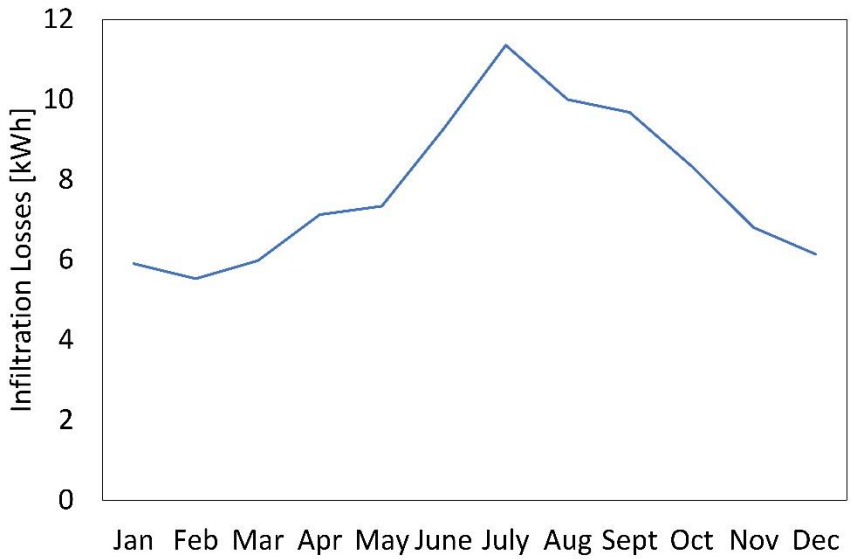

b)

Figure 11. Monthly electricity absorbed by the refrigeration unit, produced by the PV system and reintegration from the grid (a) and monthly infiltration losses during the unloading operations of the products in each delivery (b).

Fig. 12 shows the economic and $CO_{2,e}$ savings compared with the same van without PV panels. As it is seen, there is a yearly economic saving of about 138 €. Undoubtedly the savings would be of no minor importance for longer trips and carrying out more than one delivery per day. Moreover, like in the single delivery scenario, a higher cost saving should be expected with an increasing unit cost of methane.

Besides the financial information, from the environmental point of view, it is possible to save about 463.6 $kgCO_{2,e}$ per year, being more noticeable than the peak in the spring and summer months. Since the economic and environmental savings are caused by the increase of energy produced by the PV panels, similar trends are observed. Moreover, the results could further improve considering longer trips and carrying out more than one multiple-deliveries per day.

Preprints (www.preprints.org) | NOT PEER-REVIEWED | Posted: 6 June 2022 doi:10.20944/preprints202206.0088.v1

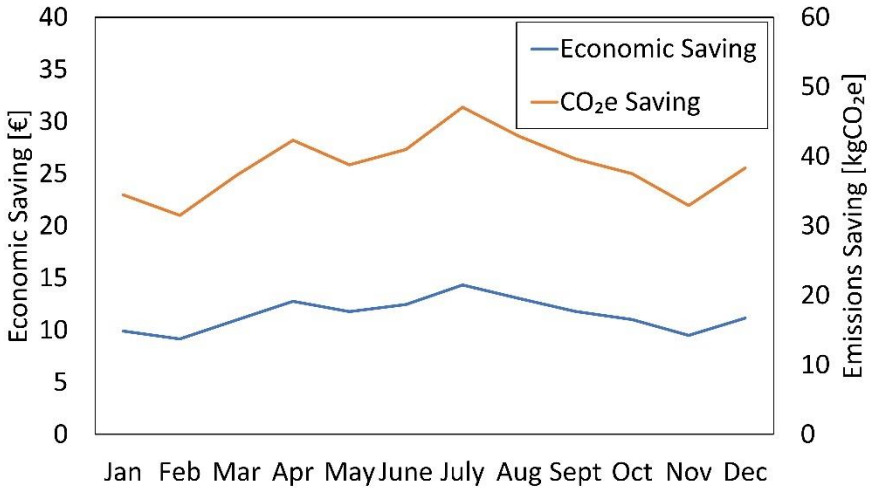

Figure 12. Monthly economic and CO_2 emissions savings provided considering the multiple-deliveries scenario. The refrigerated van represents the reference solution without the PV panels installed.

4. Conclusions

The refrigerated transport sector demands a sustainable transition to decrease the dramatic figures in total greenhouse gas emissions. Current solutions aim to the electrification of vehicles, including batteries onboard. This paper presents a comprehensive energy model (thermal-electrical) that simulates a hybrid refrigerated van and calculates fuel energy consumption, costs, and CO_2,e emissions for any type of use.

The model uses the set-point temperature, battery and photovoltaic panels characteristics, and trip as input parameters. Then, the V-I characteristic curve of the photovoltaic panels and the environmental conditions are determined. The thermal model of the refrigerated cabin, and the electrical model, including batteries and photovoltaic panels, are coupled.

For the economic analysis, all technologies produce comparable electricity annually, and the factor that determines the most suitable panel is the investment cost. Then, regarding batteries, lead-acid battery highlighted over lithium as the most convenient technology, also optimizing the capacity.

The total net savings for a single delivery scenario is around 100 € per year, and 150 to 250 kgCO_2,e emissions are avoided. In a multiple deliveries scenario, the yearly economic saving is increased to 138 €, and the carbon footprint is reduced by 464 kgCO_2,e. The batteries and the photovoltaic production are not enough to provide the cooling required by the refrigeration unit.

The hybridization of refrigerated vans can decrease carbon emissions along the cold chain. Still, their optimal design is crucial since the investment costs can hinder the transition to these eco-friendlier systems. Future works should be addressed to test alternative scenarios with different operating conditions and adopted technologies.

Author Contributions: A.M. conceived the idea, and helped with the development of the methodology and the discussion of the results. A.M.B. wrote the draft of the paper and helped with the discussion of the results. F.P. developed the thermal model, helped develop the comprehensive model, ran some simulations, and analyzed the results. M.G.D.D helped with the finalization of the manuscript and the discussion of the results. A.A. helped develop the comprehensive model, running some simulations and analyzing the results. C.A. supervised the entire work.

Funding: This research received no external funding.

Acknowledgments: Adrián Mota-Babiloni acknowledges grant IJC2019-038997-I funded by MCIN/AEI/10.13039/501100011033.

Conflicts of Interest: The authors declare no conflict of interest.

Preprints (www.preprints.org) | NOT PEER-REVIEWED | Posted: 6 June 2022 doi:10.20944/preprints202206.0088.v1

Appendix A - Refrigerated van and PV system features

The characteristics of the refrigerated van are shown in Table 1.

Table 1. Main characteristics of the refrigerated van.

Parameter	Characteristics
Engine (F1CFA401A)	4-stroke Bi-fuel spark ignition (petrol-methane) maximum power (methane): 100 kW (136 CV) @ 2730 - 3500 rpm maximum torque (methane): 350 N·m @ 1500 - 2730 rpm Displacement: 2998 cm^3
Refrigerated cabin	Reinforced isothermal class F (thermal transmittance of the walls between 0.29 and 0.4 W $m^{-2}K^{-1}$), minimum temperature inside the cabin of −20 °C
Refrigeration unit	R-452A refrigerant, hermetic compressor with inverter (30 to 80 Hz)
Refrigeration unit power supply	Electric mains or dedicated auxiliary alternator, directly driven by the heat engine

Then, the internal composition of the refrigerated cabin walls considered in the model is shown in Table A2.

Table 2. Characteristics of different materials considered for the walls.

Parameter	Body	Polyure-thane	Glass fiber reinforced polymer (GRFP)
Heat transfer transmit-tance, λ (W m^{-1} K^{-1})	60	0.024	0.64
Width, s (m)	0.005	0.064	0.002
Density, ϱ (kg m^{-3})	2700	40	1800
Specific heat capacity, c (J kg^{-1} K^{-1})	900	1400	1255

Table A3 shows the nominal characteristics of the three photovoltaic panels simulated in the energy model.

Table 3. Characteristics of each type of photovoltaic panel simulated within the energy model.

Parameter	Type A	Type B	Type C
Technology	HJT	Monocrystalline	Monocrystalline
Peak power [W]	120	108	52
V_{oc} [V]	17.3	15.3	10.9
V_{mp} [V]	14	12.6	9.1
i_{mp} [A]	8.6	8.6	5.7
i_{sc} [A]	9	9	6
Dimensions [mm]	1046x683	1046x683	1109x293
Weight [kg]	1.7	1.7	0.8

The size of the inverter was chosen according to the peak load. Its main characteristics are presented in Table A4.

Table 4. Inverter characteristics.

Parameter	Value
Nominal power [VA/W]	3000 / 3000
Voltage [VAC]	230
AC Voltage regulation (battery mode) [VAC]	230 ±5% (For Personal Computers) 170-280

Preprints (www.preprints.org) | NOT PEER-REVIEWED | Posted: 6 June 2022 doi:10.20944/preprints202206.0088.v1

	280 (For Home Appliances)
Peak power [VA]	6000
Efficiency peak [/]	90% to 93%
Transfer time [ms]	10 (For Personal Computers) 20 (For Home Appliances)
Waveshape	PURE WAVE
Battery/charge voltage [VDC]	24 / 27
Overcharge protection [VDC]	33
Type of charge controller	MPPT
Maximum capacity PV [W]	1500
Maximum PV array open-circuit voltage [VDC]	145
PV Array MPPT Voltage Range [VDC]	30 to 115
Maximum charge current: solar and AC / rest [A]	60 / 120
Relative humidity	5% to 95%
Operating /storage temperature [°C]	−10 to 50 / −15 to 60

Moreover, 95% and 90% efficiency have been assumed for the DC-DC and DC-AC conversions, respectively. Therefore, a small percentage of losses (10%) caused by the continuous DC-AC conversion is added to the net electrical power required by the refrigeration unit in monthly operation and the losses in the wiring. The remaining significant losses (about 30%) are due to the conversion between DC-AC current, including the power factor (cosφ of 0.7).

Appendix B

Table B1 summarizes the equations regarding the heat transfer mechanisms considered in the thermal model.

Table 1. Heat transfer in the refrigerated van.

Type of heat transfer	Equation
Convective between the walls external surface and the external air [30]	$\dot{Q}_{e-w} = h_e S_e [T_{amb} - T_{w-e}(x=0)]$
Convective between the walls external surface and the air inside the driver's cabin [30]	$\dot{Q}_{c-w} = h_c S_c [T_c - T_{w-c}(x=0)]$
Incident solar radiation [30]	$\dot{Q}_{rad} = \sum_{i=1}^{4} \alpha_B \, G_i S_i$
Radiative with the celestial vault (the vehicle is considered a small convex object placed inside a cavity) [30]	$\dot{Q}_{w-sky} = \sigma \varepsilon_B S_{roof} \left[T_{sky}^4 - T_{w-ext}(x=0)^4\right]$
Convective between the internal air and the surface of the inner wall bordering the outside	$\dot{Q}_{in-w} = h_{in-w} S_{in-e} [T_{w-e}(x=s_{wall}) - T_{in}]$
Convective heat exchange between the internal air and the walls inner surface bordering the driver's cabin	$\dot{Q}_{i-c} = h_{in-c} S_{in-c} [T_{w-c}(x=s_{wall}) - T_{in}]$
Internal due to the auxiliaries	$\dot{Q}_{aux}$

Preprints (www.preprints.org) | NOT PEER-REVIEWED | Posted: 6 June 2022 doi:10.20944/preprints202206.0088.v1

	$\dot{Q}_{door} = \dot{m}_a(j_{a,0} - j_{a,in})$ where,
Door opening (≠0 only in the goods loading/unloading phases, known duration) [31]	$\dot{m}_a = \left[C_{inf} S_{door} \sqrt{H} \left(\frac{\rho_{in} - \rho_e}{2}\right)^{0.5} \left[\frac{2}{1 + \left(\rho_{in}/\rho_e\right)^{1/3}}\right]^{3/2}\right] \left(\frac{\rho_{in} + \rho_e}{2}\right)$
Defrost system, given by electrical resistances (≠ 0 only during activation, known duration)	$\dot{Q}_{defrost} = 867\ W$
Cooling capacity of the refrigeration system	$\dot{Q}_{RU}$

The Fourier equation for unsteady 1D conduction is solved for the exchange with the ambient and the driver's cabin, assuming the cold room to a parallelepiped, Equation (B1).

$$\boldsymbol{\rho c \frac{\partial T_w}{\partial t} = \lambda \frac{\partial^2 T_w}{\partial x^2}}. \quad \text{(B1)}$$

The boundary conditions assumed for this model are shown in Table B2.

Table 2. Boundary conditions.

Condition	Equation
With the ambient	$-\lambda \frac{\partial T_{w-e}}{\partial x}_{x=0} = h_e[T_{amb} - T_{w-e}(x=0)] + \frac{\dot{Q}_{rad} + \dot{Q}_{w-sky}}{S_e}$
With the cabin	$-\lambda \frac{\partial T_{w-c}}{\partial x}_{x=0} = h_c[T_c - T_{w-c}(x=0)]$
With the internal air (wall that exchanges with the ambient)	$-\lambda \frac{\partial T_{w-e}}{\partial x}_{x=s_{wall}} = h_{in}[T_{w-e}(x=s_{wall}) - T_{in}]$
With the internal air (wall that exchanges with the driver's cabin)	$-\lambda \frac{\partial T_{w-c}}{\partial x}_{x=s_{wall}} = h_{in}[T_{w-c}(x=s_{wall}) - T_{in}]$
Between two adjacent layers of the stratigraphy (i and j)	$-\lambda_i \frac{\partial T_w}{\partial x}_{x=s_i^-} = -\lambda_j \frac{\partial T_w}{\partial x}_{x=s_i^+}$

The presence of the panels is modeled by a thermal energy balance with lumped parameters, Equation (B2).

$$\boldsymbol{m_{PV} c_{PV} \frac{\partial T_{PV}}{\partial t} = \dot{Q}_{rad,PV} + h_e S_{roof}(T_{amb} - T_{PV}) + h_{AG} S_{roof}(T_{AG} - T_{PV}) + \dot{Q}_{AG}}, \quad \text{(B2)}$$

where $\boldsymbol{m_{PV}}$ and $\boldsymbol{c_{PV}}$ are the mass and the specific heat of the panel, $\boldsymbol{T_{PV}}$ is the panel temperature, assumed as constant, $\boldsymbol{h_e}$ is the convective heat exchange coefficient of the ambient air, and $\boldsymbol{h_{AG}}$ of the air flowing through the interspace (AG, Air Gap), $\boldsymbol{T_{AG}}$ is the air temperature in the cavity, assumed as constant and equal to the external temperature $\boldsymbol{T_{amb}}$, $\boldsymbol{\dot{Q}_{rad,PV}}$ is the radiative heat exchange due to solar radiation and heat exchange with the celestial vault, as defined above, $\boldsymbol{\dot{Q}_{AG}}$ is the radiative heat exchange between the lower surface of the panel and the external surface of the wall, calculated as Equation (B3) indicates.

$$\boldsymbol{\dot{Q}_{AG} = \frac{\sigma S_{roof}\left(T_{roof(0)}^4 - T_{PV}^4\right)}{\frac{1}{\alpha_{front}} + \frac{1}{\alpha_{back}} - 1}}. \quad \text{(B3)}$$

The boundary condition for the roof is then determined by employing Equation (B4) and (B5).

$$\boldsymbol{-\lambda_B \frac{\partial T_w}{\partial x}_{x=0} = h_{AG}\left(T_{AG} - T_{roof}(0)\right) - \dot{q}_{AG}}, \quad \text{(B4)}$$

Preprints (www.preprints.org) | NOT PEER-REVIEWED | Posted: 6 June 2022 doi:10.20944/preprints202206.0088.v1

$$\dot{q}_{AG} = \frac{\dot{Q}_{AG}}{S_{roof}}. \quad \text{(B5)}$$

The properties of the PV panels are defined in Table B3.

Table 3. Thermodynamic and geometrical properties of the PV panels.

Density (ρ_{PV})	Width (s_{PV})	Specific heat capacity (c_{PV})	Absorptivity (front side) (α_{front})	Absorptivity (back side) (α_{back})	Emissivity (ε)
2700 kg m^{-3}	0.003 m	900 J kg^{-1} K^{-1}	0.72	0.2	0.91

Appendix C

Lithium battery

The equation representative of the lithium battery discharge is Equation (C1) [32]. Two corrective parameters $Corr_R$ and $Corr_K$ have been introduced, which allow considering a variation of the internal resistance as the battery charge varies (it) and the variation of the bias constant as the discharge current varies (i). These parameters are calculated using an optimization function that minimizes the mean square error between the two curves (simulated and real) at a given current value. An average and a maximum error of 0.4% and 1% are obtained.

$$V_b = \overline{V} - K \cdot \frac{Q}{Q-it} \cdot (it + i^*) - R \cdot i + A \cdot e^{-B \cdot it}, \quad \text{(C1)}$$

$$R = R_{ref}(1 + Corr_R \cdot it), \quad \text{(C2)}$$

$$K = K_{ref}(1 - Corr_K \cdot i), \quad \text{(C3)}$$

where:

- $\overline{V}$ is the constant voltage of the battery [V];
- K is the Polarization constant [V A^{-1}h^{-1}] or Polarization resistance [Ω];
- Q is the battery capacity [Ah];
- it is the actual charge of the battery [Ah];
- A is the width of the exponential area [V];
- B is the constant of time in the exponential area [Ah^{-1}];
- R is the internal resistance of the battery [Ω];
- i is the current [A];
- i^* is the filtered current [A].

For the charge instead, Equation (C4) is used. The polarisation resistance varies in the charging phase model and the current direction. This ends with an increase in voltage at the end of the charging process. From a mathematical point of view, it behaves like a vertical asymptote so that, at a particular state of charge, the voltage will tend to infinity.

$$V_b = \overline{V} - K \cdot \frac{Q}{Q-it} \cdot it - K \cdot \frac{Q}{it+0.05Q} \cdot i^* - R \cdot i + A \cdot e^{-B \cdot it}. \quad \text{(C4)}$$

Note that the charging process occurs in two phases, the first phase at constant current and a phase at a constant voltage. The charger will limit the current not exceeding a voltage limit value in the constant voltage phase. This phenomenon is modeled using a current limiting function where a higher current would cause an overvoltage than the chosen limiting voltage.

Lead-acid battery

For the lead-acid battery discharging phase, the variability of capacitance with current according to Peukert's law has been added. The model is valid for any SOC value.

Preprints (www.preprints.org) | NOT PEER-REVIEWED | Posted: 6 June 2022 doi:10.20944/preprints202206.0088.v1

$$V_b = \bar{V} - K \cdot \frac{Q}{Q - it} \cdot it - K \cdot \frac{Q}{Q - it} \cdot i^* - R \cdot i + Exp(t), \quad \text{(C5)}$$

$$Q(i) = \left(\frac{i}{i_{ref}}\right)^a \cdot Q_{nom}, \quad \text{(C6)}$$

$$a = \frac{\log(Q(i_2)) - \log(Q(i_1))}{\log(i_1) - \log(i_2)}, \quad \text{(C7)}$$

where:

- $Q(i)$ is the battery capacity, in Ah, at the discharge current i;
- Q_{nom} is the nominal battery capacity at a reference discharge current i_0;
- $Q(i_2)$ and $Q(i_1)$ are two different battery capacities at different discharge rates i_2 and i_2;
- $Exp(t)$ is the exponential voltage [V], given by:

$$Exp(t) = B \cdot |i(t)| \cdot (-Exp(t) + A \cdot u(t)), \quad \text{(C8)}$$

with variable $u(t)$ in charge ($u(t) = 1$) or discharge mode ($u(t) = 0$).

A new control phase has been added to the model for the charging phase. A map of values allows identifying the maximum currents supplied according to the SOC and the limit voltage to be charged. Therefore, currents that cause an overvoltage in the constant voltage charging phase are limited.

$$V_b = \bar{V} - K \cdot \frac{Q}{Q - it} \cdot it - K \cdot \frac{Q}{Q - 0.1\,it} \cdot i^* - R \cdot i + Exp(t) \quad \text{(C9)}$$

The limits imposed by the model are that: the minimum no-load battery voltage is 0 V, while the maximum battery voltage is 2 $\bar{V}$ and the minimum battery capacity is 0 Ah, and the maximum capacity is Q. Therefore, the maximum SOC cannot exceed 100% if the battery is overcharged.

It is possible to obtain the necessary parameters using the manual supplied with the batteries. The characteristic discharge curve is provided together with the internal resistance R of the battery. The characteristic time constant of the filtered current i^* can be obtained through experimental tests or assumed equal to 10s (a value considered acceptable by the literature for both lithium and lead-acid batteries). The calculated values for the discharge phase are also used to model the charge phase.

The state of charge (percentage of residual charge) is given by the following equation [33]:

$$SOC(t) = SOC(0) + \frac{\eta_i \int_0^t i(t)dt}{Q}. \quad \text{(C10)}$$

The efficiency η_i is the Coulombic efficiency, with a unitary value in the case of discharge and less than one in the case of charge (variable according to the type of battery).

The slow dynamics of voltage adjustment for an instantaneous step change of the current is modeled by the filtered current i * flowing through the bias resistor:

$$\frac{i - i^*}{\tau} = \frac{di^*}{dt}, \quad \text{(C11)}$$

with τ representing the characteristic time constant of the considered battery.

The model can simulate the experimental voltage with a good approximation, with an error below 5% throughout the charging process.

Generalization of the model

The two types of battery considered so far have been modeled considering a 12V 100Ah battery so that all the parameters refer to this battery size. To obtain the capacity

Preprints (www.preprints.org) | NOT PEER-REVIEWED | Posted: 6 June 2022 doi:10.20944/preprints202206.0088.v1

and voltage of a generically sized battery, it is necessary to identify generalized parameters.

For a generic capacity:

$$\boldsymbol{Q_{conv}} = \frac{\boldsymbol{Q_{ref}}}{\boldsymbol{Q_{nom}}}, \tag{C12}$$

where Q_{conv} is a conversion parameter obtained as the ratio between the reference capacity (in this case, 100 Ah) and the nominal capacity of the battery that we want to adopt.

By the same reasoning, the correction parameters and the internal resistance are:

$$\boldsymbol{Corr_R} = \frac{\boldsymbol{Corr_{R,ref}}}{\boldsymbol{Q_{conv}}}, \tag{C13}$$

$$\boldsymbol{Corr_K} = \frac{\boldsymbol{Corr_{K,ref}}}{\boldsymbol{Q_{conv}}}, \tag{C14}$$

$$\boldsymbol{R} = \boldsymbol{R_{ref}} * \boldsymbol{Q_{conv}}. \tag{C15}$$

For a generic voltage:

$$\boldsymbol{V_{conv}} = \frac{\boldsymbol{V_{ref}}}{\boldsymbol{V_{nom}}}, \tag{C16}$$

$$\boldsymbol{R} = \frac{\boldsymbol{R_{ref}}}{\boldsymbol{V_{conv}}}. \tag{C17}$$

So, for a generic voltage and a generic capacity:

$$\boldsymbol{R} = \frac{\boldsymbol{R_{ref}}}{\boldsymbol{V_{conv}}} * \boldsymbol{Q_{conv}}. \tag{C18}$$

References

1. UNECE Climate Change and Sustainable Transport.
2. Lawton, R.; Curlin, J.S.; Clark, W. *TECHNOLOGY BRIEF IIR-UN Environment Cold Chain Brief on Transport Refrigeration*; 2018;
3. Rai, A.; Tassou, S.A. Energy demand and environmental impacts of alternative food transport refrigeration systems. *Energy Procedia* **2017**, *123*, 113–120, doi:10.1016/J.EGYPRO.2017.07.267.
4. Ladha-Sabur, A.; Bakalis, S.; Fryer, P.J.; Lopez-Quiroga, E. Mapping energy consumption in food manufacturing. *Trends Food Sci. Technol.* 2019, *86*, 270–280.
5. Yang, Z.; Tate, J.E.; Morganti, E.; Shepherd, S.P. Real-world CO2 and NOX emissions from refrigerated vans. *Sci. Total Environ.* **2021**, *763*, 142974, doi:10.1016/j.scitotenv.2020.142974.
6. Sovacool, B.K.; Bazilian, M.; Griffiths, S.; Kim, J.; Foley, A.; Rooney, D. Decarbonizing the food and beverages industry: A critical and systematic review of developments, sociotechnical systems and policy options. *Renew. Sustain. Energy Rev.* 2021, *143*, 110856.
7. Mota-Babiloni, A.; Makhnatch, P. Predictions of European refrigerants place on the market following F-gas regulation restrictions. *Int. J. Refrig.* **2021**, *127*, 101–110, doi:https://doi.org/10.1016/j.ijrefrig.2021.03.005.
8. Li, G. Comprehensive investigation of transport refrigeration life cycle climate performance. *Sustain. Energy Technol. Assessments* **2017**, *21*, 33–49, doi:10.1016/j.seta.2017.04.002.
9. Citarella, B.; Viscito, L.; Mochizuki, K.; Mauro, A.W. Multi-criteria (thermo-economic) optimization and environmental analysis of a food refrigeration system working with low environmental impact refrigerants. *Energy Convers. Manag.* **2022**, *253*, 115152, doi:10.1016/j.enconman.2021.115152.
10. Górny, K.; Stachowiak, A.; Tyczewski, P.; Zwierzycki, W. Lubricity of selected oils in mixtures with the refrigerants R452A, R404A, and R600a. *Tribol. Int.* **2019**, *134*, 50–59, doi:10.1016/j.triboint.2018.12.033.

11. Nasuta, D.; Srichai, R.; Zhang PhD, M.; Martin, C.; Muehlbauer, J. Life Cycle Climate Performance Model for Transport Refrigeration/Air Conditioning Systems. *ASHRAE Trans.* **2014**, *120*, 8–1P,2P,3P,4P,5P,6P,7P,8P.
12. Tassou, S.A.; De-Lille, G.; Ge, Y.T. Food transport refrigeration - Approaches to reduce energy consumption and environmental impacts of road transport. *Appl. Therm. Eng.* **2009**, *29*, 1467–1477, doi:10.1016/j.applthermaleng.2008.06.027.
13. Wu, X.; Hu, S.; Mo, S. Carbon footprint model for evaluating the global warming impact of food transport refrigeration systems. *J. Clean. Prod.* **2013**, *54*, 115–124, doi:10.1016/J.JCLEPRO.2013.04.045.
14. Cenex *Refrigerated Transport Insights - A ZERO White Paper*; Loughborough (UK), 2021;
15. Njoroge, P.; Ndunya, L.S.; Kabiru, P. Hybrid Solar-Wind Power System for Truck Refrigeration. *2018 IEEE PES/IAS PowerAfrica* **2018**, 1–9.
16. Blasko, V.; Bendapudi, S.; Oggianu, S.M. Solar power assisted transport refrigeration systems, transport refrigeration units and methods for same 2013, *1*, 1–15.
17. Sarbu, I.; Sebarchievici, C. Review of solar refrigeration and cooling systems. *Energy Build.* **2013**, *67*, 286–297, doi:https://doi.org/10.1016/j.enbuild.2013.08.022.
18. Lazzarin, R.M. Solar cooling: PV or thermal? A thermodynamic and economical analysis. *Int. J. Refrig.* **2014**, *39*, 38–47, doi:https://doi.org/10.1016/j.ijrefrig.2013.05.012.
19. Infante Ferreira, C.; Kim, D.-S. Techno-economic review of solar cooling technologies based on location-specific data. *Int. J. Refrig.* **2014**, *39*, 23–37, doi:https://doi.org/10.1016/j.ijrefrig.2013.09.033.
20. Kim, D.S.; Infante Ferreira, C.A. Solar refrigeration options – a state-of-the-art review. *Int. J. Refrig.* **2008**, *31*, 3–15, doi:https://doi.org/10.1016/j.ijrefrig.2007.07.011.
21. Salilih, E.M.; Birhane, Y.T. Modelling and performance analysis of directly coupled vapor compression solar refrigeration system. *Sol. Energy* **2019**, *190*, 228–238, doi:10.1016/j.solener.2019.08.017.
22. Su, P.; Ji, J.; Cai, J.; Gao, Y.; Han, K. Dynamic simulation and experimental study of a variable speed photovoltaic DC refrigerator. *Renew. Energy* **2020**, *152*, 155–164, doi:https://doi.org/10.1016/j.renene.2020.01.047.
23. Mahmoudi, M.; Dehghan, M.; Haghgou, H.; Keyanpour-Rad, M. Techno-economic performance of photovoltaic-powered air-conditioning heat pumps with variable-speed and fixed-speed compression systems. *Sustain. Energy Technol. Assessments* **2021**, *45*, 101113, doi:10.1016/j.seta.2021.101113.
24. Novaes Pires Leite, G. de; Weschenfelder, F.; Araújo, A.M.; Villa Ochoa, Á.A.; Franca Prestrelo Neto, N. da; Kraj, A. An economic analysis of the integration between air-conditioning and solar photovoltaic systems. *Energy Convers. Manag.* **2019**, *185*, 836–849, doi:https://doi.org/10.1016/j.enconman.2019.02.037.
25. Lazzarin, R.M.; Noro, M. Past, present, future of solar cooling: Technical and economical considerations. *Sol. Energy* **2018**, *172*, 2–13, doi:https://doi.org/10.1016/j.solener.2017.12.055.
26. Reda, F.; Paiho, S.; Pasonen, R.; Helm, M.; Menhart, F.; Schex, R.; Laitinen, A. Comparison of solar assisted heat pump solutions for office building applications in Northern climate. *Renew. Energy* **2020**, *147*, 1392–1417, doi:https://doi.org/10.1016/j.renene.2019.09.044.
27. Riva, C.; Roumpedakis, T.C.; Kallis, G.; Rocco, M. V; Karellas, S. Life cycle analysis of a photovoltaic driven reversible heat pump. *Energy Build.* **2021**, *240*, 110894, doi:https://doi.org/10.1016/j.enbuild.2021.110894.
28. Barth, M..; Younglove, T..; Scora, G. Development of a Heavy-Duty Diesel Modal Emissions and Fuel Consumption Model. *UC Berkeley Calif. Partners Adv. Transp. Technol. Retrieved from https//escholarship.org/uc/item/67f0v3zf* **2005**.
29. Meneghetti, A.; Ceschia, S. Energy-efficient frozen food transports: the Refrigerated Routing Problem. *Int. J. Prod. Res.* **2020**, *58*, 4164–4181, doi:10.1080/00207543.2019.1640407.
30. Torregrosa-Jaime, B.; Bjurling, F.; Corberán, J.M.; Di Sciullo, F.; Payá, J. Transient thermal model of a vehicle's cabin validated under variable ambient conditions. *Appl. Therm. Eng.* **2015**, *75*, 45–53,

 doi:10.20944/preprints202206.0088.v1

doi:10.1016/j.applthermaleng.2014.05.074.

31. Stoecker, W.F. Industrial Refrigeration Handbook. *McGraw-Hill Educ. - Eur.* **1998**.
32. Tremblay, O.; Dessaint, L.A. Experimental validation of a battery dynamic model for EV applications. *24th Int. Batter. Hybrid Fuel Cell Electr. Veh. Symp. Exhib. 2009, EVS 24* **2009**, *2*, 930–939.
33. Chang, W.-Y. The State of Charge Estimating Methods for Battery: A Review. *ISRN Appl. Math.* **2013**, *2013*, 1–7, doi:10.1155/2013/953792.